Electronic Supplementary Information

Experimental Section

Materials: All reagents used in this work are analytical grade. Cupric nitrate hexahydrate ($Cu(NO_3)_2 \cdot 6H_2O$), hydrochloric acid (HCl), ammonium chloride (NH_4Cl)，sulfuric acid (H_2SO_4), were purchased from Kelong chemically(Chengdu, China). Polyvinyl alcohol (PVA, Mw = 67000), Polytetrafluoroethylene (PTFE, 60 wt% of solid content), Sodium nitrate ($NaNO_3$), sodium nitrite ($NaNO_2$), sodium nitroferricyanide dihydrate($C_5FeN_6Na_2O \cdot 2H_2O$), sodium salicylate($C_7H_5NaO_3$), salicylic acid ($C_7H_6O_3$), trisodium citrate dihydrate ($C_6H_5Na_3O_7 \cdot 2H_2O$), sodium hypochlorite solution (NaClO), pp-dimethylamino benzaldehyde($C_9H_{11}NO$), 0.8 wt% sulfamic acid solution (H_3NO_3S), were purchased from Aladdin Ltd (Shanghai, China). Nafion solution (5 wt%) was purchased from Sigma-Aldrich Chemical Reagent Co., and Ltd. Deionized water was purified through a Millipore system.

Preparation of catalysts: Cu@CNFs was prepared by the electrospinning method. Firstly, 0.3 g of $Cu(NO_3)_2 \cdot 6H_2O$, 1.5 g of PVA were dissolved in 10 mL of water under vigorous stirring at 90 °C for 180 min. 2 g of PTFE was then added into the solution. Subsequently, the prepared solution was moved to a syringe with a stainless-steel nozzle. A high-voltage of 21 kV was supplied and the distance between the needle tip and the rotating drum collector is 22 cm. After electrospinning, the asspun fibres were collected and heat-treated at 280 °C for 2 h in air. The fiber was heated in argon at 2 $^{o}C\ min^{-1}$ to 400 ^{o}C, then at 1$^{o}C\ min^{-1}$ to 500 ^{o}C and kept warm for 1h, and finally at 600 ^{o}C for 2h to form Cu@CNFs. CNFs were prepared using the same

procedure, except without the addition of copper salts.

Material characterizations： X-ray diffraction (XRD) analysis of the samples was performed by Rigaku Ultima IV X-ray diffractometer with Cu Kα radiation. The sample morphology was photographed by ZEISS Sigma 360 scanning electron microscope. The acceleration voltage was 3 kV during topography shooting and 15 kV during energy spectrum mapping shooting. The detector is SE2 secondary electronic detector. The transmission electron microscopy (TEM) and high-resolution TEM (HRTEM) images of sample were obtained using JEOL JEM-200F equipment with the accelerating voltage of 300 kV. The ion chromatography (IC) was tested by Thermo Scientific ICS-900. The Differential Electrochemical Mass Spectrometry (DEMS) measurements were performed on the Linglu QAS 100.

Working electrode preparation: 5 mg catalyst were grinded into powder and added into a mixed solution containing 660 μL ethanol, 300 μL deionized water and 40 μL of 5 wt% Nafion solution, followed by 30 min ultrasonic dispersion to form a homogeneous suspension. Then, 20 μL of such suspension was dropped on carbon paper (CP, 1×1cm^2), and dried at ambient temperature.

Electrochemical measurements: All electrochemical measurements were performed in a hydrogen cell equipped with a Nafion membrane in the middle. The experiments were conducted using a three-electrode system. The working electrode was a carbon sheet coated with the catalyst, the counter electrode was a platinum tablet, and the reference electrode was a saturated Ag/AgCl/KCl electrode. The electrolyte for both the anode and cathode was 0.1 M PBS (prepared from Na_2HPO_4 and NaH_2PO_4), which

is a neutral electrolyte with a pH of 7. Sodium nitrate ($NaNO_3$) was added to the high-temperature, purified electrolyte as a nitrogen source.

In 0.1 M PBS with 0.1 M $NaNO_3$ electrolyte, the voltage of the relative reference electrode (Ag/AgCl) was converted into the voltage of the relatively reversible hydrogen electrode (RHE) by formula (1):

$$E(RHE) = 0.0591 \times PH + E\left(\frac{Ag}{AgCl}\right) + 0.197V \quad (1)$$

In this experiment, the pH value of electrolyte is tested at 6.85.

The linear sweep voltammetry (LSV) was performed to compare the presence and absence of nitrate salts in the same electrolyte at a scan rate of 5 mV s^{-1}. Under non-Faradaic current conditions, cyclic voltammetry (CV) experiments were carried out at scan rates of 100 mV s^{-1}, 120 mV s^{-1}, 140 mV s^{-1}, 160 mV s^{-1}, 180 mV s^{-1}, and 200 mV s^{-1} in the potential range from 0.5 V to 0.6 V vs Ag/AgCl. Electrochemical impedance spectroscopy (EIS) was employed to measure the solution resistance within a frequency range of 0.01 to 10 kHz.

Determination of ammonia (NH_3): Ammonia produced in the NITRR process was colored by indophenol blue method and detected by the UV-vis spectroscopy. Due to the high concentration of the product, all electrolytes after electrolysis were diluted 20 times before color development. After 1 hour of electrolysis, the electrolyte was diluted 20 times to 2 mL, followed by 2 mL colorant (containing salicylic acid, sodium citrate and sodium hydroxide), 1 mL of oxidant (0.05 M sodium hypochlorite), and 0.2 mL of catalyst solution (1 wt% sodium nitroferricyanide). Then, they were placed in the dark environment for 2 h, and the UV-vis spectra were measured in the wavelength

range of 550 ~ 800 nm. The absorption intensity at 655 nm was substituted into the standard curve to quantify the ammonia yield. Calibration of NH_4Cl standard solutions with different concentrations was carried out, and the fitting curve was calculated as $y=0.42336x+0.01339$. ($R^2=0.99943$).

Determination of Nitrite (NO_2^-): The nitrite concentration was measured using the Griess reagent. To prepare the Griess reagent, 0.2 g of N-(1-naphthyl) ethyl-enediamine dihydrochloride, 2.0 g of sulfanilamide, and 5.88 mL of phosphoric acid were dissolved in 100 mL of deionized water and stirred thoroughly. This formed the Griess reagent. After electrolysis, the electrolyte was diluted 10 times, and then 1 mL of the Griess reagent and 2 mL of deionized water were added. 1 mL of the diluted electrolyte was taken and allowed to react in the dark at room temperature for 20 minutes, during which the solution developed a magenta color. The absorbance was measured using a UV-Vis spectrophotometer in the 400-650 nm range, and the absorbance at 540 nm was recorded. The nitrite concentration was determined by comparing the absorbance value at 540 nm to a standard calibration curve. The calibration of $NaNO_2$ standard solutions with different concentrations was carried out, and the fitting curve was calculated as $y=0.2195x+0.02132$. ($R^2=0.99943$).

Detection of hydrogen (H_2): In the NITRR process, there is a competing reaction, the Hydrogen Evolution Reaction (HER), occurring at the cathode. Since H_2 is a product of the HER, it can be detected by passing the electrolysis products into a gas chromatograph (GC) through the cathode chamber. To minimize experimental errors caused by differences in the thermal conductivity of gases, nitrogen was used as the

carrier gas for the chromatograph. Nitrogen was introduced into the cathode electrolyte at a flow rate of 20 mL min^{-1}, and the GC collected the gas produced by the reaction in the cathode chamber every 5 minutes. By integrating the characteristic peak of hydrogen detected by the thermal conductivity detector (TCD), the concentration of hydrogen can be determined.

Calculations of faradaic efficiency (FE) and yield rate:

The FE of NH_3 is calculated by equation (2):

$$NH_3\ FE = \frac{8 \times F \times c(NH_3) \times V}{17 \times Q} \times 100\%$$

(2)

The FE of NO_2^- is calculated by equation (3):

$$NO_2^-\ FE = \frac{2 \times F \times c(NO_2^- \times V)}{46 \times Q} \times 100\%$$

(3)

The yield of NH_3 is calculated by equation (4):

$$NH_3\ yield\left(\mu g\ h^{-1}\ mg_{cat.}^{-1}\right) = \frac{c(NH_3) \times V}{t \times m_{cat.}} \quad (4)$$

The yield of NH_3 is calculated by equation (5):

$$NO_2^-\ yield\left(\mu g\ h^{-1}\ mg_{cat.}^{-1}\right) = \frac{c(NO_2^-) \times V}{t \times m_{cat.}} \quad (5)$$

The concentration of H_2 is measured by GC and TCD. The volume mole number n can be calculated according to formula (6):

$$n = \frac{P \times V(H_2)}{RT} \quad (6)$$

The corresponding FE of H_2 can be calculated by equation (7):

$$H_2FE = \frac{2 \times F \times n}{Q} \times 100\% \quad (7)$$

c (mg h^{-1} $mg^{-1}_{cat.}$): the measured NH_3/NO_2^- concentration. V: the volume of electrolyte in the cathode chamber. t: the time for which the potential is applied. F: Faraday constant (F=96485 C mol^{-1}). $m_{cat.}$: the mass of catalyst loaded on the working electrode. Q: the charge applied. P: the standard atmospheric pressure. V(H_2): volume of hydrogen generated by GC test. R: the universal gas constant. T: the reaction temperature.

Differential Electrochemical Mass Spectrometry (DEMS) measurements:

The 0.1 M $NaNO_3^-$based PBS solution was pumped into the electrochemical cell using a peristaltic pump. Prior to and during the DEMS test, argon (Ar) was continuously bubbled into the electrolyte at a flow rate of 0.8 mL/min. A carbon paper coated with Cu@CNFs electrocatalyst was used as the working electrode, a platinum wire as the counter electrode, and Ag/AgCl as the reference electrode. The experiment began with a linear sweep voltammetry (LSV) scan from 0.4 V vs. RHE to –1.4 V vs. RHE at a scan rate of 10 mV s^{-1}. The scan continued until the baseline stabilized, and then the corresponding mass signals were collected. After the electrochemical test, once the mass signal returned to the baseline, the next cycle was performed under the same conditions to avoid any experimental errors. The DEMS test was completed after six cycles.

Computational methods

First-principles calculations were performed within the density functional theory framework.[1] The projector-augmented wave (PAW) method[2,3] and the generalized

gradient approximation (GGA)[4] for the exchange-correlation energy functional, as implemented in the Vienna ab initio simulation package (VASP)[5-8] were used. The GGA calculation was performed with the Perdew-Burke-Ernzerhof (PBE)[9] exchange-correlation potential. Considered long-range interaction between molecules/intermediates and surface, Van der Waals interactions were considered using DFT-D3 correlation. [10] To avoid effects come from other slabs, a vacuum of 15 Å was added along z direction. The convergence criterion of geometry relaxation was set to 0.03 eV·Å^{-1} in force on each atom. The energy cutoff for plane wave-basis was set to 600 eV. The K points were sampled with 3×3×1 by Monkhorst-Pack method. The change in free energy (ΔG) of per reaction step was calculated as following :[11]

$$\Delta G = \Delta E + \Delta \mathrm{ZPE} - \mathrm{T}\cdot\Delta S + \Delta G_{\mathrm{U}} + \Delta G_{\mathrm{pH}}$$

Where ΔE is the change of the total reaction energy obtained from DFT calculation, ΔZPE is the change of the zero-point energy, T is the temperature (300 K), and ΔS is the change of the entropy. $\Delta G_{\mathrm{U}} = -\mathrm{eU}$, where U is the potential at the electrode and e is the transferred charge. $\Delta G_{\mathrm{pH}} = k_B \cdot T \times \ln 10 \times \mathrm{pH}$, where k_B is the Boltzmann constant and T = 300 K. In this work, the influence of pH was neglected. The Cu surface model in the calculations was determined to be the (200) plane based on the experimental TEM results (Fig. 1c). The heterostructure model (Cu@CNF) is constructed by combining Cu (200) and C planes, with the (√3×√3) R30° transformation applied exclusively to the C plane to ensure lattice constant matching.[12]

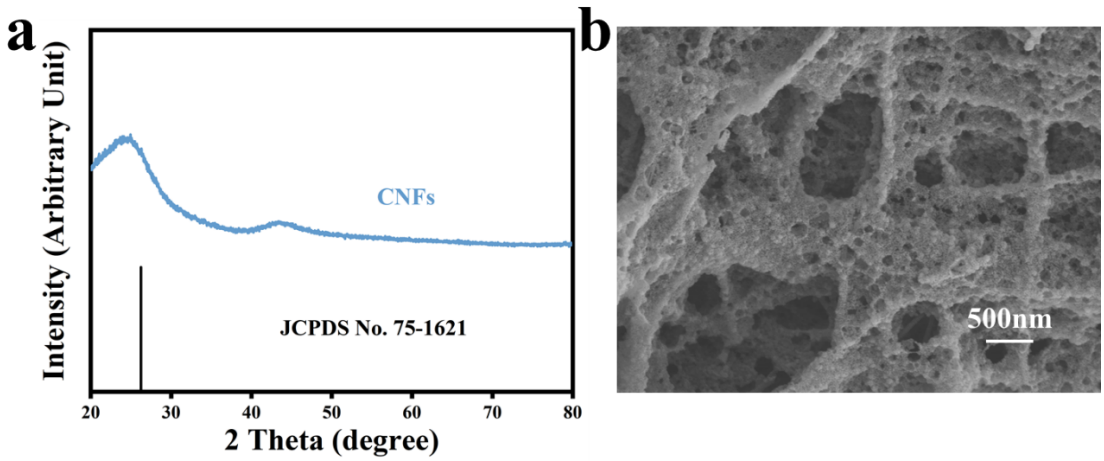

Fig. S1. (a) XRD pattern and (b) SEM image of CNFs.

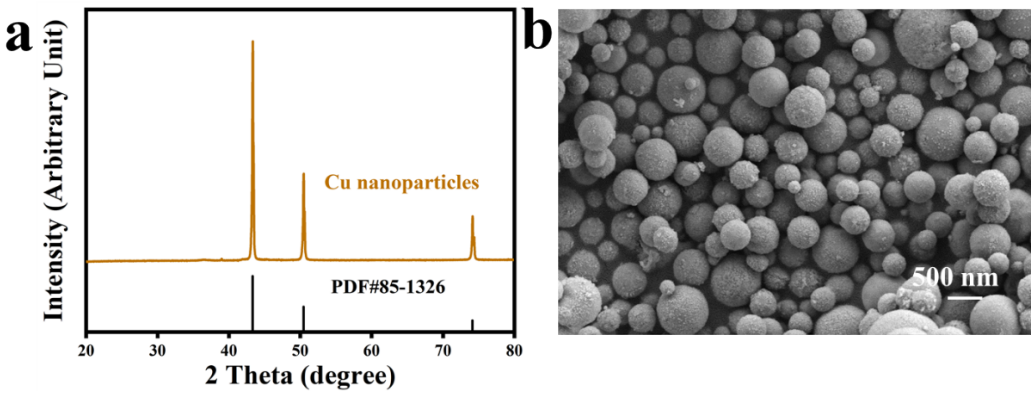

Fig. S2. (a) XRD pattern and (b) SEM image of commercial Cu nanoparticles

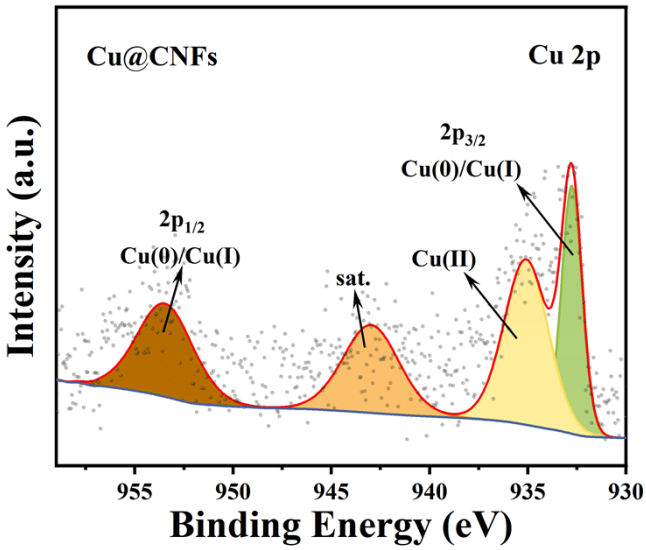

Fig. S3. XPS spectra of Cu@CNFs in the Cu 2p

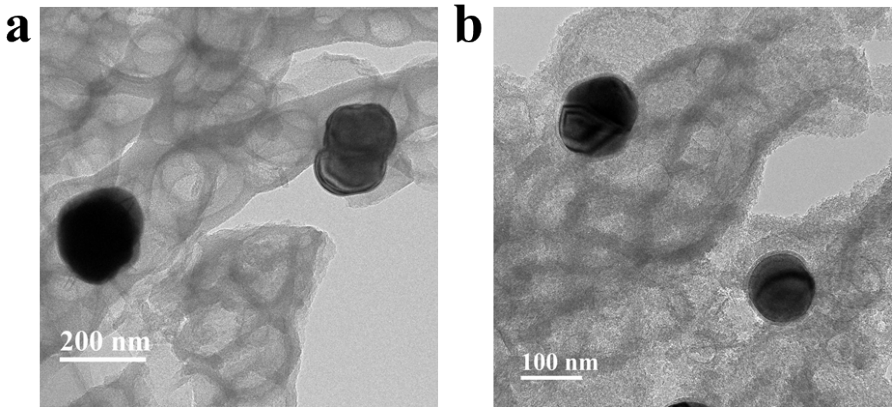

Fig. S4. TEM image of Cu@CNFs.

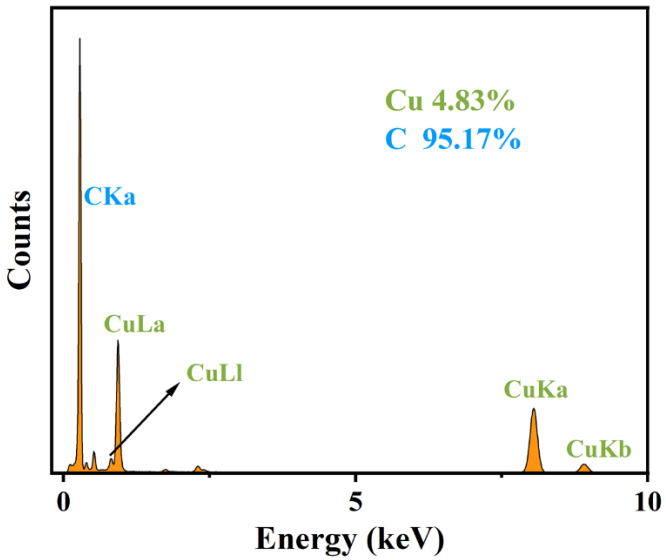

Fig. S5. EDX spectra for Cu@CNFs

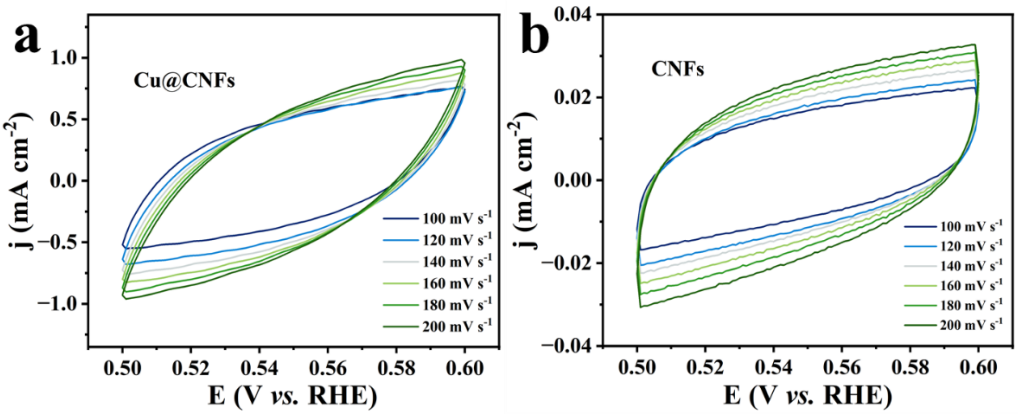

Figure S6. Cyclic Voltammetry (CV) curves of Cu@CNFs and CNFs at five different scan rates from 100 to 200 mV s^{-1}.

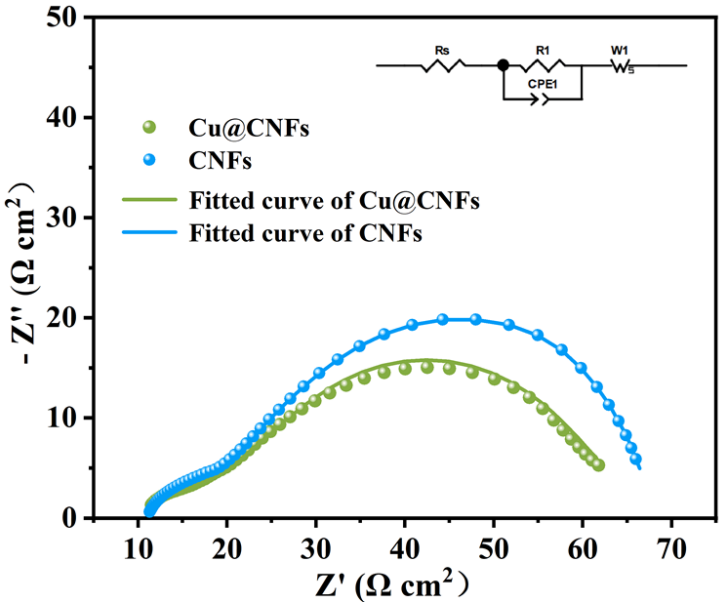

Figure S7. EIS of Cu@CNFs and CNFs.

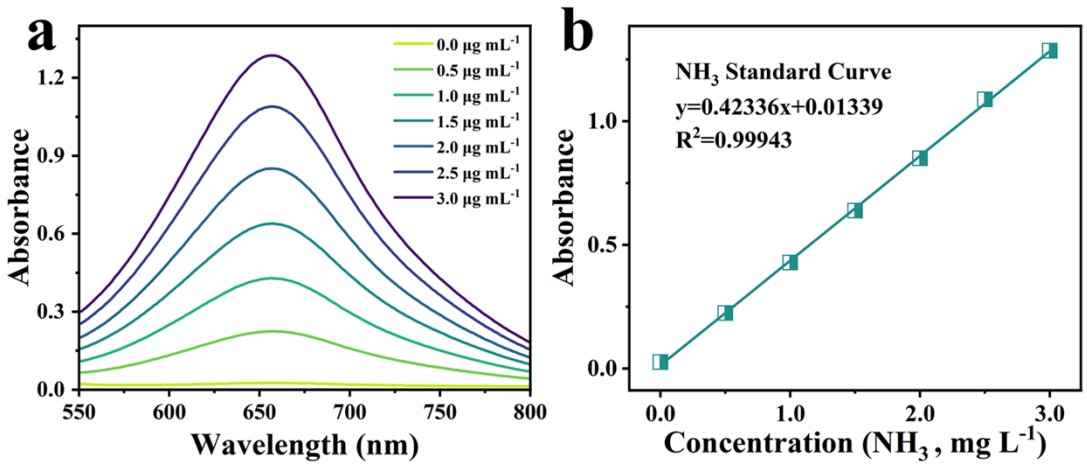

Figure S8. (a) UV-vis absorption spectra of different concentrations of NH_3 stained with indophenol blue and (b) the corresponding calibration curve in 0.1 M PBS.

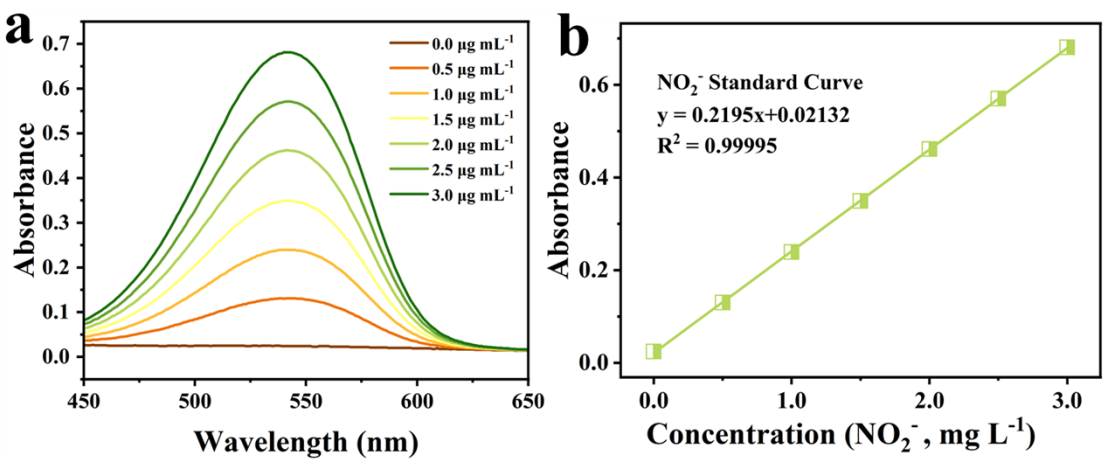

Fig. S9. (a) UV-vis absorption spectra of various concentrations of NO_2^- after sitting for 20 minutes and (b) the corresponding calibration curve in 0.1 M PBS.

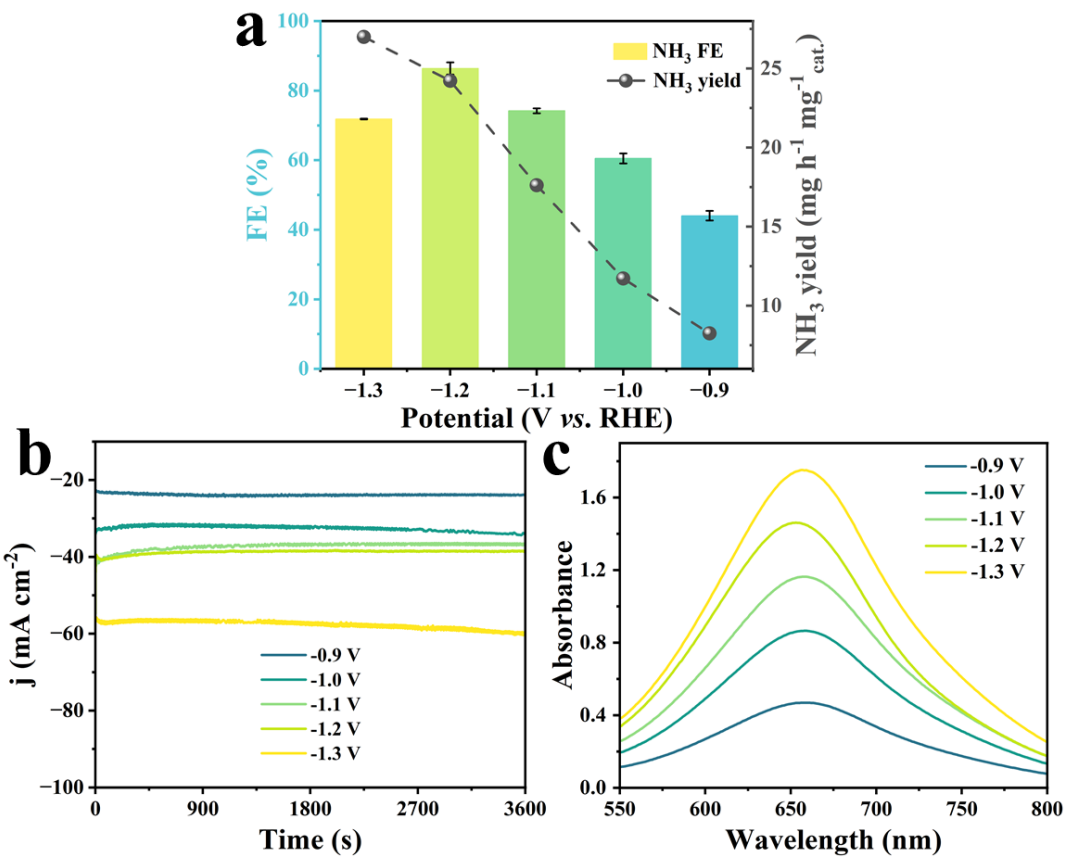

Fig. S10. (a) NH_3 FE and NH_3 yields of Cu@CNFs at different applied potentials. (b) Chronoamperometry curves of Cu@CNFs at various potentials during 1 h of electrolysis in 0.1 M PBS with 0.1 M NO_3^-. (c) UV–Vis absorption spectra at 5 various potentials with the indophenol indicator of Cu@CNFs.

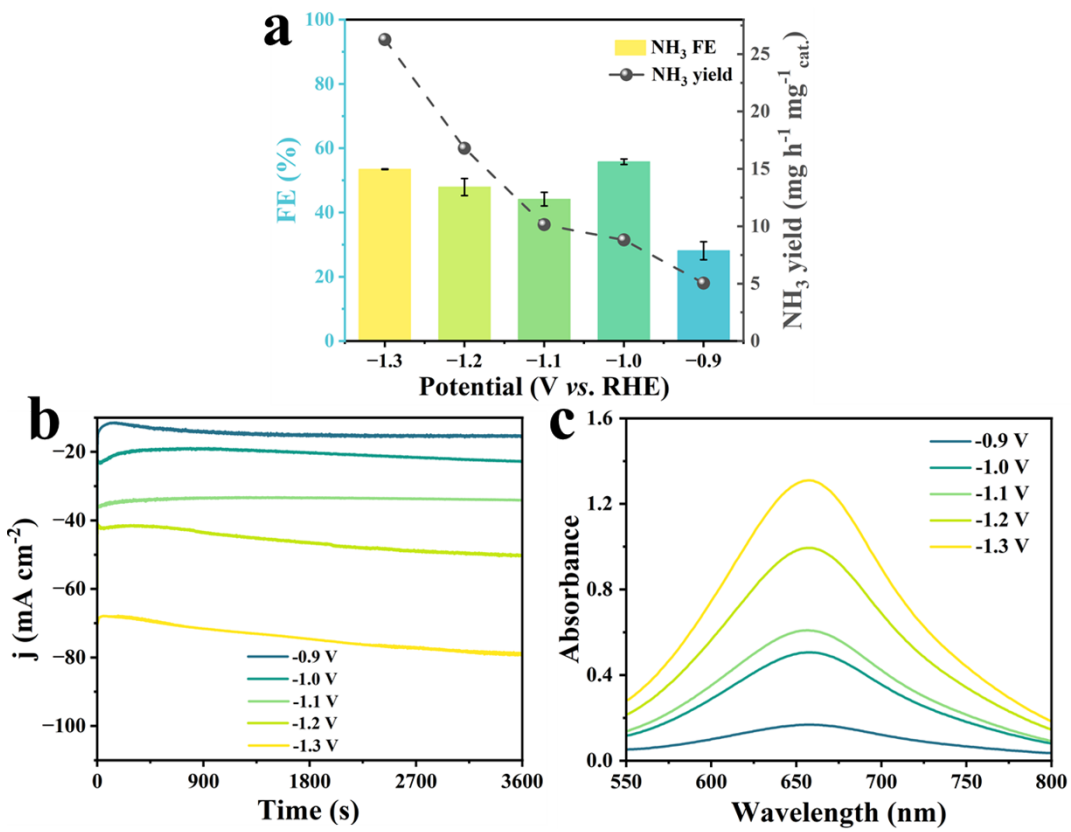

Fig. S11. (a) NH_3 FE and NH_3 yields of CNFs at different applied potentials. (b) Chronoamperometry curves of CNFs at various potentials during 1 h of electrolysis in 0.1 M PBS with 0.1 M NO_3^-. (c) UV–Vis absorption spectra at 5 various potentials with the indophenol indicator of CNFs.

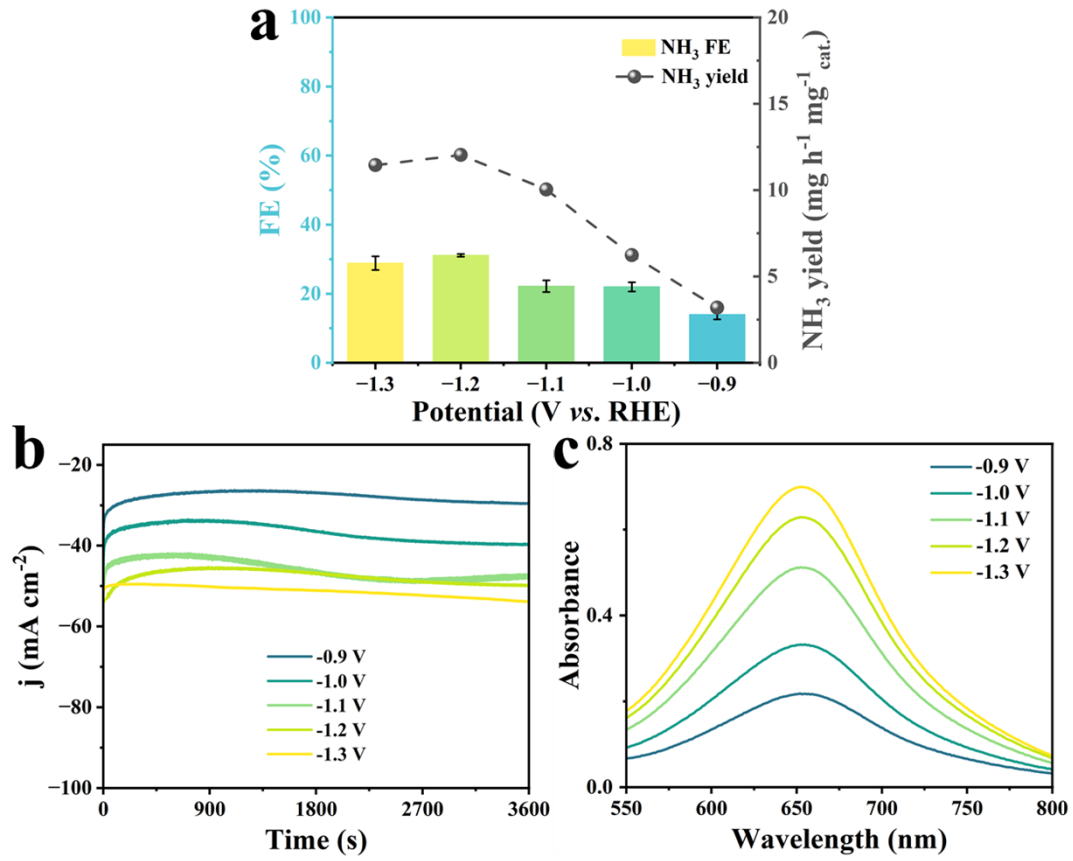

Fig. S12. (a) NH_3 FE and NH_3 yields of Cu nanoparticles at different applied potentials. (b) Chronoamperometry curves of Cu nanoparticles at various potentials during 1 h of electrolysis in 0.1 M PBS with 0.1 M NO_3^-. (c) UV–Vis absorption spectra at 5 various potentials with the indophenol indicator of CNFs.

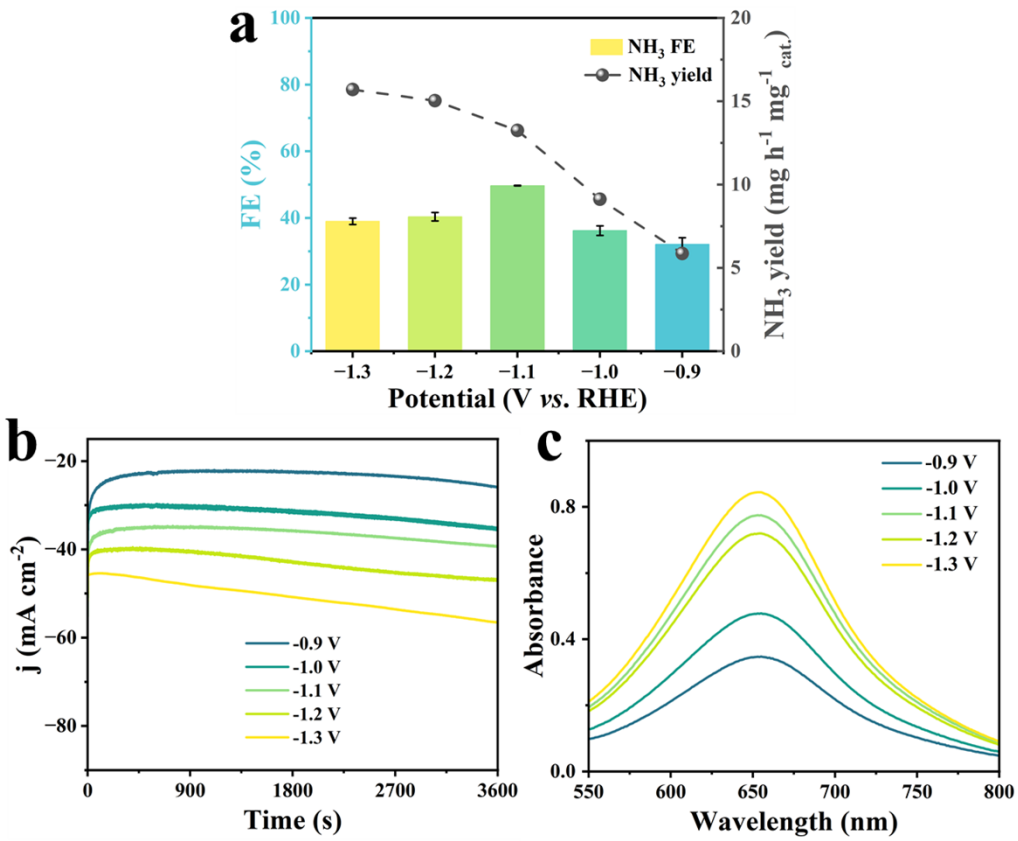

Fig. S13. (a) NH_3 FE and NH_3 yields of Cu nanoparticles mixed with CNFs at different applied potentials. (b) Chronoamperometry curves of Cu nanoparticles mixed with CNFs at various potentials during 1 h of electrolysis in 0.1 M PBS with 0.1 M NO_3^-. (c) UV–Vis absorption spectra at 5 various potentials with the indophenol indicator of Cu nanoparticles mixed with CNFs.

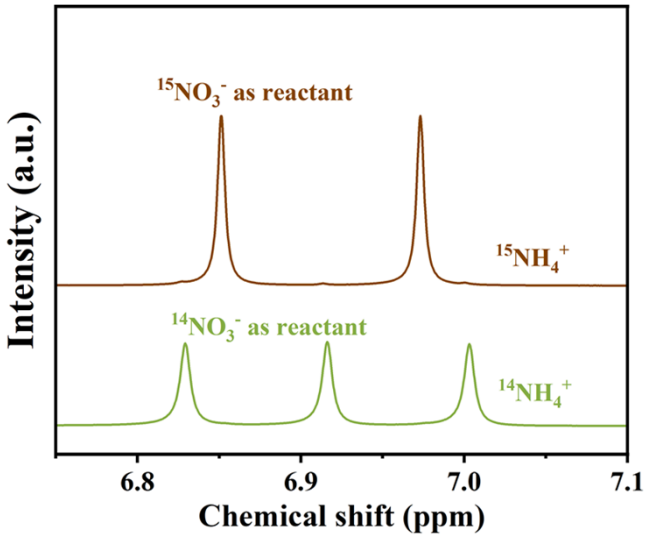

Fig. S14. ^{1}H NMR spectra of electrolyte after NitRR using $^{15}NO_3^-$ and $^{14}NO_3^-$ as nitrogen sources, respectively

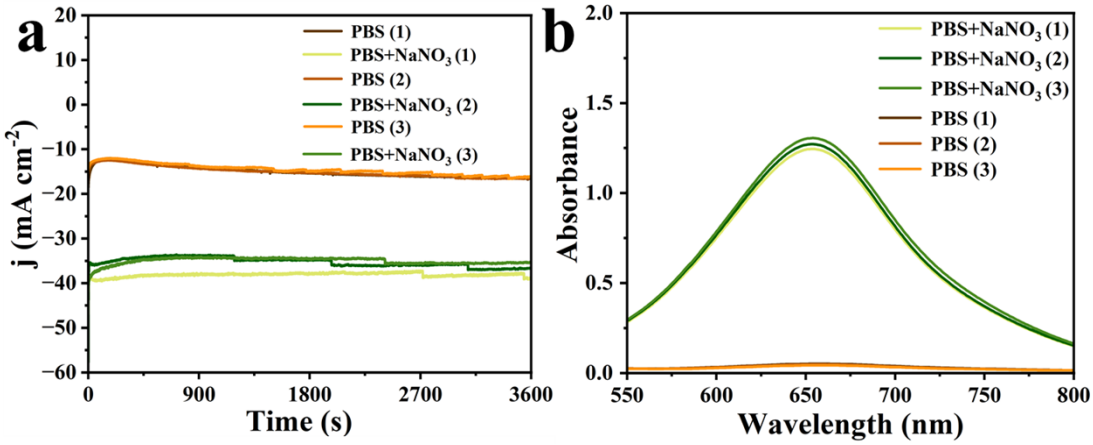

Fig. S15. (a) i-t curves for 1 h. (b) UV-vis absorption spectra of NH_3 with alternating 1h cycles in the PBS electrolyte with and without NO_3^- for Cu@CNFs.

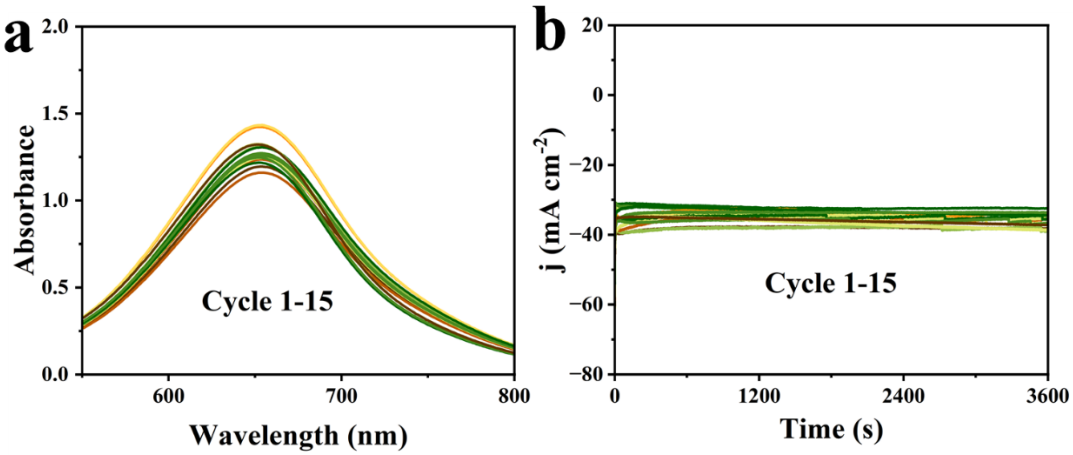

Fig. S16. (a) i-t curves for 1 h. (b) UV-vis absorption spectra of NH_3 of each cycle.

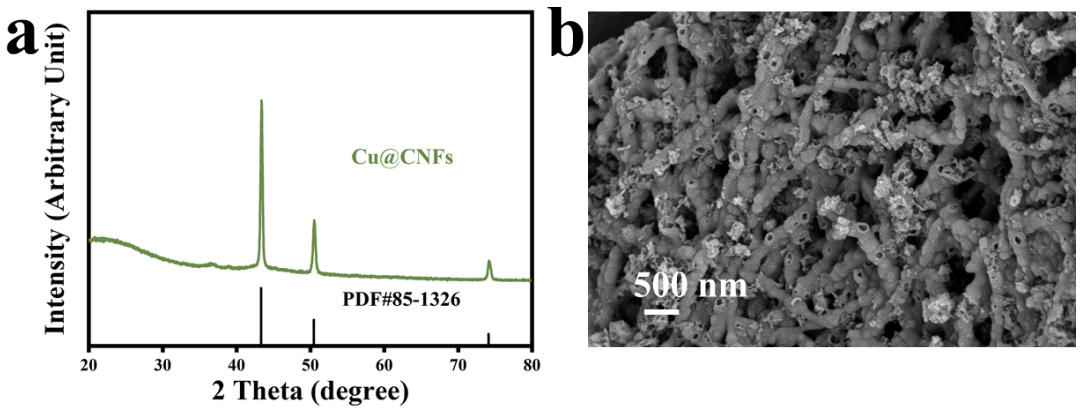

Fig. S17. (a) XRD pattern of Cu@CNFs after calcination. (b) SEM image of Cu@CNFs after calcination.

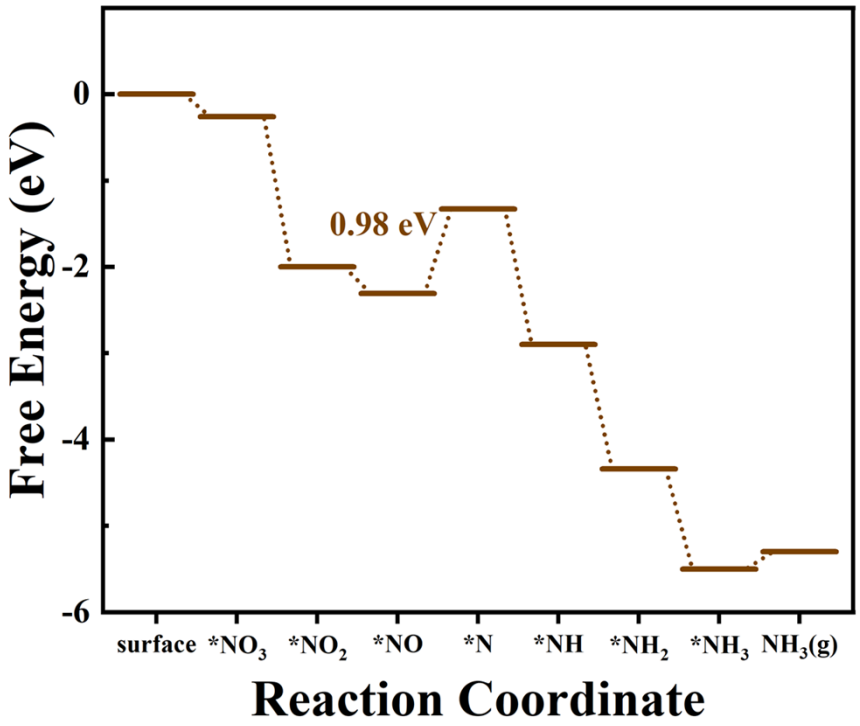

Fig. S18. The free energy diagram of NitRR process on the Cu (200) surface.

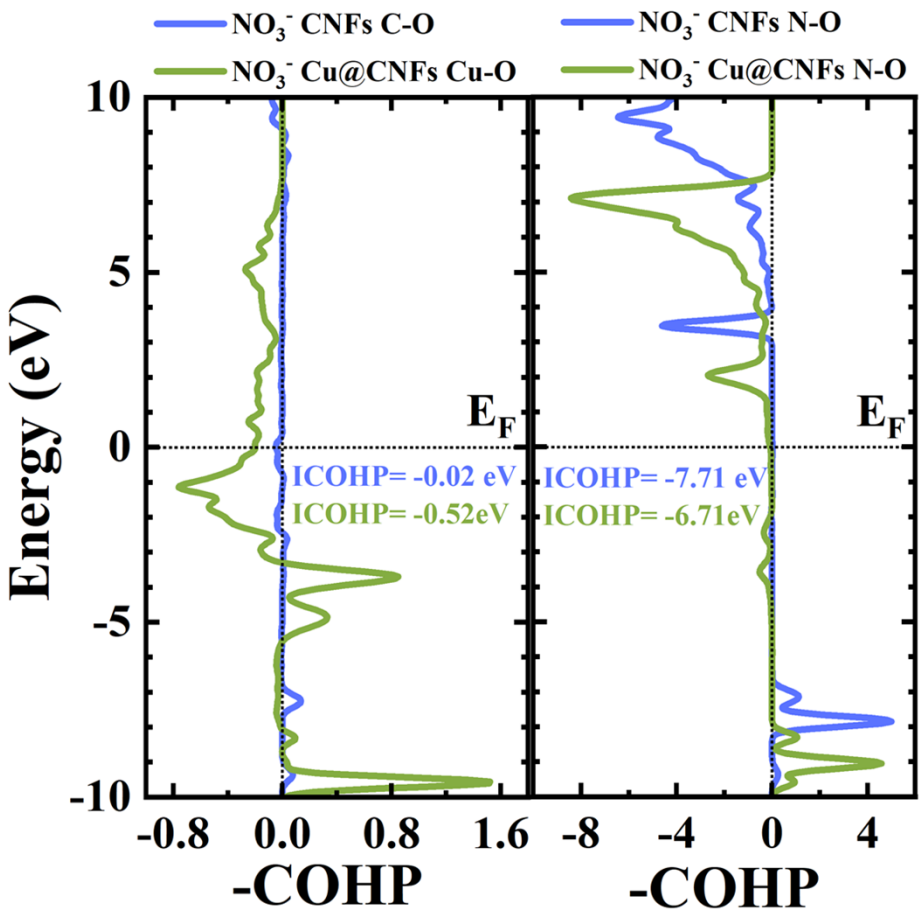

Fig. S19. The COHP of the bonds between (a) the active site (C/Cu) and O atom of NO_3^- group. (b) the N and O atoms of NO_3^- group. The values of corresponding ICOHP are marked in the image.

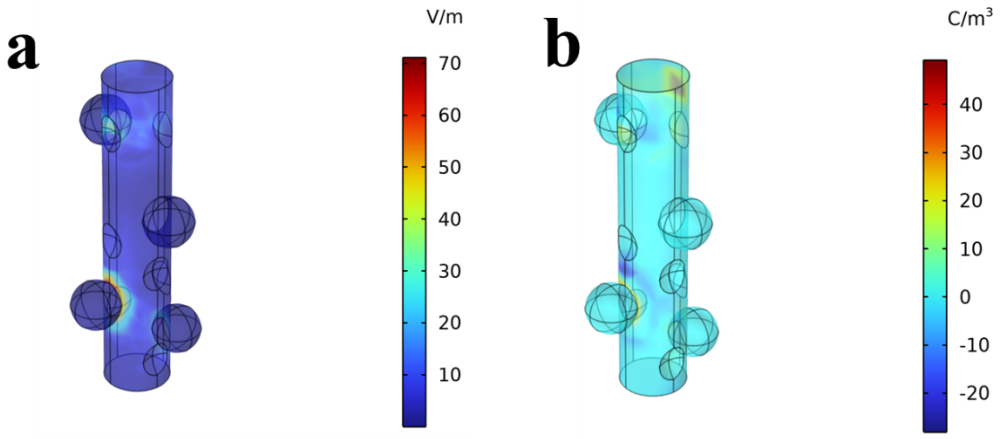

Fig. S20. (a) Electric field density and (b) charge density simulation results for Cu@CNFs.

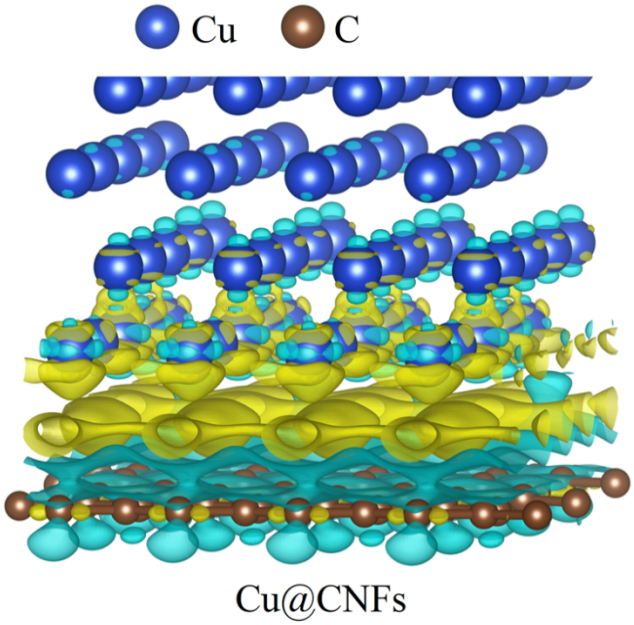

Fig. S21. The charge density difference for the formation of Cu and CNF.

Table S1. Comparison of electrocatalytic NitRR performance for Cu@CNFs with other electrocatalysts under ambient conditions.

Catalysts	Electrolyte	Potential(V)	FE	NH_3 yield	Ref.
Cu@CNFs	**0.1 M PBS with 0.1 M $NaNO_3$**	**–1.2 V**	**86.38%**	**24.22 mg h^{-1} $mg^{-1}_{cat.}$**	**This work**
Mo_2C	0.5 M Na_2SO_4, 0.1 M NO_3^-	–0.6	85.20%	4.8 mg cm^{-2} h^{-1}	13
PP-Co	0.1 M NaOH with 0.1 M NO_3^-	–0.6	90.10%	1.1 mmol h^{-1} $mg^{-1}_{cat.}$ (19.8 mg h^{-1} $mg^{-1}_{cat.}$)	14
Ir NTs	0.1 M $HClO_4$ with 1M NO_3^-	–0.06	84.70%	0.921 mg h^{-1} $mg^{-1}_{cat.}$	15
Fe	0.50M KNO_3, 0.10 M K_2SO_4	–0.66	76.00%	20 mg h^{-1} $mg^{-1}_{cat.}$	16
CuO_X	0.1 M KOH, 0.2 50ppm NO_3	-0.25	74.18 ±2.27%	449.41 ± 12.18 μg h^{-1} $mg^{-1}_{cat.}$	17
BCN@Cu	0.1 M KOH +100 mM NO_3^-	–0.50	89.30%	7.41 mg h^{-1} $mg^{-1}_{cat.}$	18
Cu_2O/Cu	1 M KOH + 250 mg L^{-1} NO_3^-	–0.25	79.64%	2.17 mg cm^{-2} h^{-1}	19
Fe_3O_4/SS	0.1 M NaOH + 0.1 M $NaNO_3$	–0.50	91.50%	10.145 mg cm^{-2} h^{-1}	20
10Cu/TiO_{2-x}	200 ppm NO_3^-	–0.75	81.34%	0.1143 mmol h^{-1} $mg^{-1}_{cat.}$ (2.0574 mg h^{-1} $mg^{-1}_{cat.}$)	21
Ti	0.3 M KNO_3+ 0.1 M HNO_3	–1.00	82%	3.55 mg h^{-1} $mg^{-1}_{cat.}$	22
$Ti_{0.95}Nb_{0.05}O_{2-\delta}$	0.1 M PBS with 0.1 M KNO_3	–1.35	70.64%	27.94 mg h^{-1} $mg^{-1}_{cat.}$	23
Co_3O_4@NiO HNTs	0.5M Na_2SO_4 (200 ppm NO_3^-)	–0.70	54.97%	0.12 mg h^{-1} $mg^{-1}_{cat.}$	24
Pd-NDs/Zr-MOF	0.1 M Na_2SO_4 + 500 ppmNO_3^-	–1.3	58.10%	5.17158 mg h^{-1} $mg^{-1}_{cat.}$	25

Reference:

1. W. Kohn, L.J. Sham, *Phys. Rev.*, 1965, **140**, A1133-1138.
2. P. Blöchl, *Phys. Rev. B*, 1994, **50**, 17953.
3. G. Kresse, D. Joubert, *Phys. Rev. B*, 1999, **59,** 1758-1775.
4. J. Perdew, Y. Wang, *Phys. Rev. B*, 1992, **45**, 13244-13249.
5. G. Kresse, J. Hafner, *Phys. Rev. B*, 1993, **47**, 558-561.
6. G. Kresse, J. Furthmüller, *Phys. Rev. B*, 1996, **54**, 11169.
7. L. Chen, L.Z. Zhou, H.B. Lu, Y.Q. Zhou, J.L. Huang, J. Wang, Y. Wang, X.L. Yuan, Y. Yao, *Chem. Commun.*, 2020, **56**, 9138-9141.
8. G. Kresse, J. Furthmüller, *Comput. Mater. Sci*, 1996, **6**,15-50.
9. J. Perdew, K. Burke, M. Ernzerhof, *Phys. Rev. Lett.*, 1996, **77**, 3865-3868.
10. S. Grimme, J. Antony, S. Ehrlich, H. Krieg, *J. Chem. Phys.*, 2010, **132**, 154104.
11. J. Nørskov, J. Rossmeisl, A. Logadottir, L. Lindqvist, J.R. Kitchin, T. Bligaard, H. Jonsson, *J. Phys. Chem. B*, 2004, 108, 17886-17892.
12. G. Bihlmayer, Ph. Kurz, S.Blügel, *Phys. Rev. B,*2000, **62**, 4726
13. X. Li, S. Wang, G. Wang, P. Shen, D. Ma and K. Chu, *Dalton Trans.*, 2022, **51**, 17547.
14. Q. Chen, J. Liang, Q. Liu, K. Dong, L. Yue, P. Wei, Y.Luo, Q. Liu, N. Li, B. Tang, A. A. Alshehri, M.S. Hamdy, Z. Jiang and X. Sun, *Chem. Commun.*, 2022, **58**, 4259.
15. J. Zhu, Q. Xue, Y. Xue, Y. Ding, F. Li, P. Jin, P. Chen, and Y. Chen, *ACS Appl. Mater. Interfaces,* 2020, **12**, 14064-14070.

16. Z. Wu, M. Karamad, X. Yong, Q. Huang, D. A. Cullen, P.Zhu, C. Xia , Q. Xiao, M. Shakouri , F. Chen , J.Y. Kim , Y. Xia , K. Heck , Y. Hu , M. S. Wong , Q. Li, I. Gates, S. Siahrostami and H. Wang, *Nat Commun.,* 2021, **12**, 2870.
17. J. Geng, S.Ji, H. Xu, C. Zhao, S. Zhang and H. Zhang, *Inorg. Chem. Front.*, 2021, **8**, 5209.
18. X. Zhao, G. Hu, F. Tan, S. Zhang, X. Wang, X. Hu, A. V. Kuklin, G. V.Baryshnikov, H. Agren, X. Zhou and H. Zhang, *J. Mater. Chem. A*, 2021, **9**, 23675.
19. W. Fu, Z. Hu, Y. Zheng, P. Su, Q. Zhang, Y. Jiao, M. Zhou, *Chem. Eng. J.*, 2022,**433**, 133680.
20. X. Fan, L. Xie, J. Liang, Y. Ren, L. Zhang, L. Yue, T. Li, Y. Luo, N.Li, B. Tang, Y. Liu, S. Gao, A. A. Alshehri, Q. Liu, Q. Kong and X. Sun, *Nano Res.,*2022, **15**, 3050–3055.
21. X. Zhang, C. Wang, Y. Guo, B. Zhang, Y. Wang and Y. Yu, *J. Mater. Chem. A,* 2022, **10**, 6448.
22. J. M. McEnaney, S. J. Blair, A. C. Nielander, J. A. Schwalbe, D. M. Koshy, M. Cargnello, and T. F. Jaramillo, *ACS Sustainable Chem. Eng.,* 2020, **8**, 2672-2681.
23. X.Du, K. Wang, T. Wang, H. Guo, J. Chen, J. Wang, T. Li, *Int. J. Hydrogen Energy*, 2023, **48**, 37077-37085.
24. Y. Wang, C. Liu, B. Zhang and Y.Yu, *Sci. China Mater.*, 2020, **63**, 2530–2538.
25. M. Jiang, J. Su, X. Song, P. Zhang, M. Zhu, L. Qin, Z. Tie, J. Zuo, and Z. Jin, *Nano Lett.*, 2022, **22**, 2529-2537.